# Technical Notes 10

## MINERAL LIBERATION

R P King

 

## 10 MINERAL LIBERATION

Recovery of minerals using ore dressing and concentration operations is based on methods that separate particles on the basis of their physical or chemical properties. Individual minerals can be separated completely only if each particle contains only one mineral. Two minerals in the same particle can never be separated using physical separation methods alone. Separating minerals at the particulate level is referred to as liberation since the individual minerals are liberated from each other in a physical way. In practice however, the comminution processes that are used to reduce mineralogical raw materials to the particulate state are, for the most part, unselective and, apart from a few unusual cases, the particles that are formed consist of mixtures of the mineral components that are present in the original ore.

During comminution there is, however, a natural tendency towards liberation and particles that are smaller than the mineral grains that occur in the ore can appear as a single mineral. This happens when the particle is formed entirely within a mineral grain. Obviously this will occur more frequently the smaller the particle size and it is impossible when the particle is substantially larger than the mineral grains in the ore. Typical patterns for the distribution of particles in the size-composition space are shown in Figure 2.11 in Chapter 2. Methods that can be used to model these distributions are presented in this chapter. These methods must necessarily be quite complex because the geometrical structure of any mineralogical material is not uniform and cannot be described by the familiar conventional regular geometrical entities such as spheres and cubes. Mineralogical textures have indeterminate geometries which are to a greater or lesser extent random in size, shape, orientation, and position. Likewise the particles that are generated by comminution operations are irregular in shape and size. Thus the particle population is made up of individuals that have irregular shapes and sizes and which are composed of material which itself has an irregular and complex texture of mineral phases. In spite of this lack of regularity, the distributions of particles with respect to composition do show some regular features particularly with respect to the variation of the distribution with particle size. An empirical but useful distribution is discussed in the next section.

The mineralogical scale of a mineralogical texture is difficult to specify and often the different mineral components are present in the texture at vastly different size scales. In spite of this it is useful to regard each mineral as having a characteristic size that is commensurate with the size of individual grains in the texture. It is not possible to assign a definite value to this size because every mineral grain will be different in size and shape. Except in the most regular crystalline structures, it is not possible to assign a unique size to a grain of irregular shape. In spite of this, the concept of grain size is useful in that it provides some idea of the size to which the material must be reduced by comminution in order to achieve liberation of the phase. The concept of some characteristic grain size has been used in a semi-quantitative sense for many years in mineral processing and this concept is developed here by using a hypothetical liberation size as the main parameter in the development of a quantitative model for mineral liberation during comminution. This concept was introduced in response to the observation that, for many real ore textures, the distribution of particles over the grade range changes from a distribution that is concentrated around the average grade to one that

shows considerable dispersion towards the liberated ends over a comparatively small particle size range. This effect is illustrated in Figure 2.11. This rapid change in liberation behavior is evidence that significant liberation occurs at a particle size that is characteristic for the mineral texture.

The models for liberation that are described in this chapter are specific to mineralogical textures that consist of only two minerals - a valuable species and all the other minerals that are present and which are classified as gangue minerals in any one analysis. Although the techniques that are used can be applied to multi-component ores, the details of a suitable analysis are not yet worked out and they are not included here.

## 10.1 The Beta Distribution for Mineral Liberation

A useful distribution function is developed in this section for the description of the populations of particles that have variable mineral content. This distribution function is based on the beta distribution that is widely used in mathematical statistics.

When describing a population of particles that have a distribution of mineral content, four parameters at least are essential to provide a description of the population that can be usefully used in practice. These are the average grade of the mineral, the dispersion of particle grades about the average value and in addition the fraction of particles that contain only a single mineral - one parameter for each mineral. The latter two quantities are usually referred to as the liberated ends of the distribution. If these latter two quantities are not specified the information is seriously incomplete and the resulting liberation distribution is not very useful because it does not account for the most significant particles of all, namely, those that are liberated.

The following symbols are used to represent the four parameters.
$\bar{g}$ = average grade of mineral in the population (expressed as mass fraction)
$\sigma_g$ = standard deviation about the mean in the population
$L_0$ = mass fraction of the population that consists of liberated gangue particles.
$L_1$ = mass fraction of the population that consists of liberated mineral.

The particle population is conceived as consisting of three groups; liberated particles of gangue, liberated particles of mineral and the remainder of the particles which are all composed of mixtures of the two minerals. The distribution of mineral grades over the third group is called the interior grade distribution and the beta distribution function is used as a model. The distribution density for particle grade is given by

$$p(g) = (1 - L_0 - L_1)\frac{g^{\alpha-1}(1-g)^{\beta-1}}{B(\alpha,\beta)} \qquad \text{for } 0 < g < 1 \qquad (3.1)$$

$\alpha$ and $\beta$ are two parameters that characterize the distribution and $B(\alpha,\beta)$ is the Beta function. Two Dirac delta functions must be added at each end to complete this distribution.

Some useful properties of the Beta distribution

$$\int_0^1 g^{\alpha-1}(1-g)^{\beta-1}\,dg = B(\alpha,\beta) \tag{3.2}$$

The mean of the interior distribution is given by

$$\bar{g}^M = \int_0^1 g\frac{g^{\alpha-1}(1-g)^{\beta-1}}{B(\alpha,\beta)}\,dg = \frac{B(\alpha+1,\beta)}{B(\alpha,\beta)} = \frac{\alpha}{\alpha+\beta} \tag{3.3}$$

The variance of the interior distribution is defined as

$$(\sigma^2)^M = \int_0^1 (g-\bar{g}^M)^2\,\frac{g^{\alpha-1}(1-g)^{\beta-1}}{B(\alpha,\beta)}\,dg \tag{3.4}$$

The parameters $\alpha$ and $\beta$ are related to the mean and the variance through the expressions

$$\alpha = \bar{g}^M\gamma \tag{3.5}$$

and

$$\beta = (1-\bar{g}^M)\gamma \tag{3.6}$$

where $\gamma$ is given by

$$\gamma = \frac{\bar{g}^M - (\bar{g}^M)^2 - (\sigma^2)^M}{(\sigma^2)^M} \tag{3.7}$$

Both $\alpha$ and $\beta$ must be positive numbers and therefore equations 3.5 and 3.6 require $\gamma > 0$. This in turn imposes an upper limit on the variance of the distribution by equation 3.7

$$(\sigma^2)^M < \bar{g}^M(1-\bar{g}^M) \tag{3.8}$$

The corresponding cumulative distribution is given by

$$P(g) = L_0 + (1-L_0-L_1)I_g(\alpha,\beta) \tag{3.9}$$

where $I_g(\alpha,\beta)$ is the incomplete beta function defined by

$$I_g(\alpha,\beta) = \frac{1}{B(\alpha,\beta)}\int_0^g x^{\alpha-1}(1-x)^{\beta-1}\,dx \tag{3.10}$$

The Beta distribution is sufficiently flexible to represent real particle grade distributions in a realistic way. When $\alpha = \beta$ the distribution is symmetrical about the grade g = 0.5. In practice particle grade distributions in real materials are generally asymmetric because the average grade of the valuable mineral species is often quite low. The beta distribution function is shown in Figure 3.1 for a number of combinations of the parameters $\alpha$ and $\beta$. These distributions are shown as both

distribution densities and cumulative distributions. On the cumulative distribution, the liberated mineral at each end of the distribution represented by the vertical discontinuities at $g = 0$ and $g = 1$. Note how the distribution density changes from bell-shaped to U-shaped as the variance of the inner distribution varies from 0.1 (lower graph) to 0.3 (upper graph). This is an essential requirement for the description of mineral liberation distributions for different particle sizes. When the particle size is distinctly larger than the sizes of the mineral grains within the ore, most particles in the population exhibit a mineral grade close to the mean value for the ore as a whole and the distribution is bell-shaped. On the other hand when the particle size is distinctly smaller than the sizes of the mineral grains, the tendency for liberated and nearly liberated particles to appear is greatly enhanced and the Beta distribution function reflects this tendency by exhibiting a strong U-shape. In the limit, as the variance approaches its maximum value $\bar{g}^M(1 - \bar{g}^M)$ , the Beta distribution can also describe a particle population that consists of completely liberated particles only. These properties of the Beta distribution are exploited in the following sections to develop models for the liberation process.

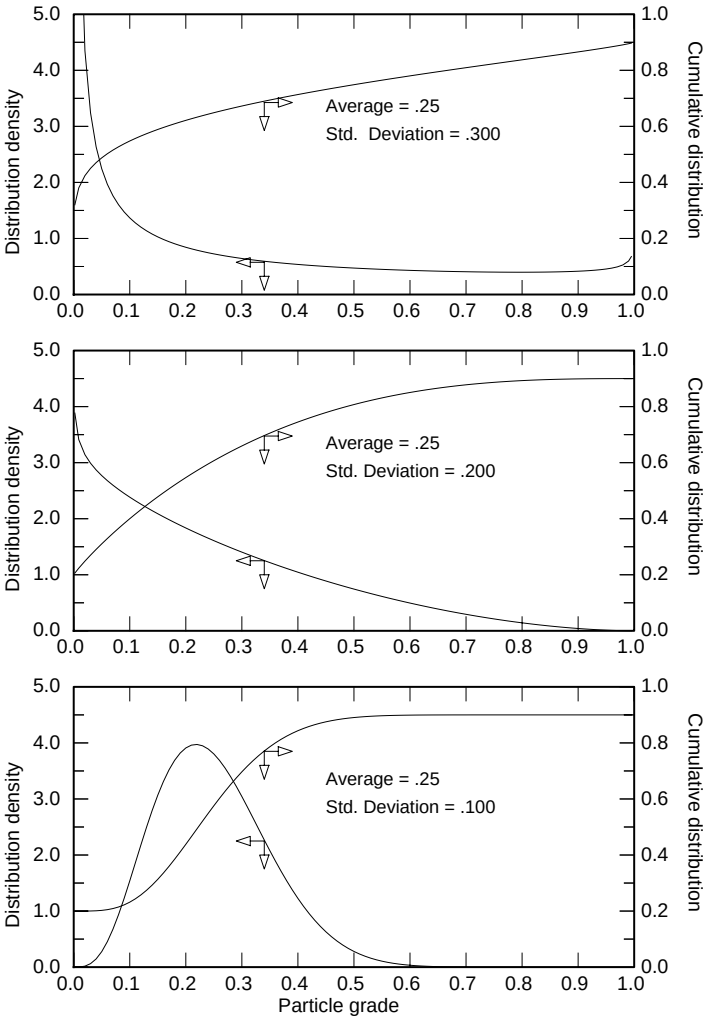


Figure 3.1 Beta distribution function for description of mineral liberation. Three cases are shown with varying values of $(\sigma^2)^M$. The distribution density changes from bell-shaped to U-shaped as the variance increases.

In practice it is common to represent the liberated material in terms of the fraction of the available mineral that is liberated

$$\begin{aligned} \mathcal{L}_1 &= \bar{g}L_1 \\ \mathcal{L}_0 &= (1 - \bar{g})L_0 \end{aligned} \tag{3.11}$$

## 10.2 **Graphical Representation of the Liberation Distribution**

The distribution density function that is described in Section 3.1 is not particularly useful for practical work. There is no convenient way of representing the liberated material at each end of the distribution density. This deficiency can be overcome by using either the cumulative distribution on which the liberated ends appear as vertical steps at each end of the graph or as a histogram that displays the distribution of particles in a finite number of grade classes. The three distributions in Figure 3.1 are shown as histograms in Figure 3.2.

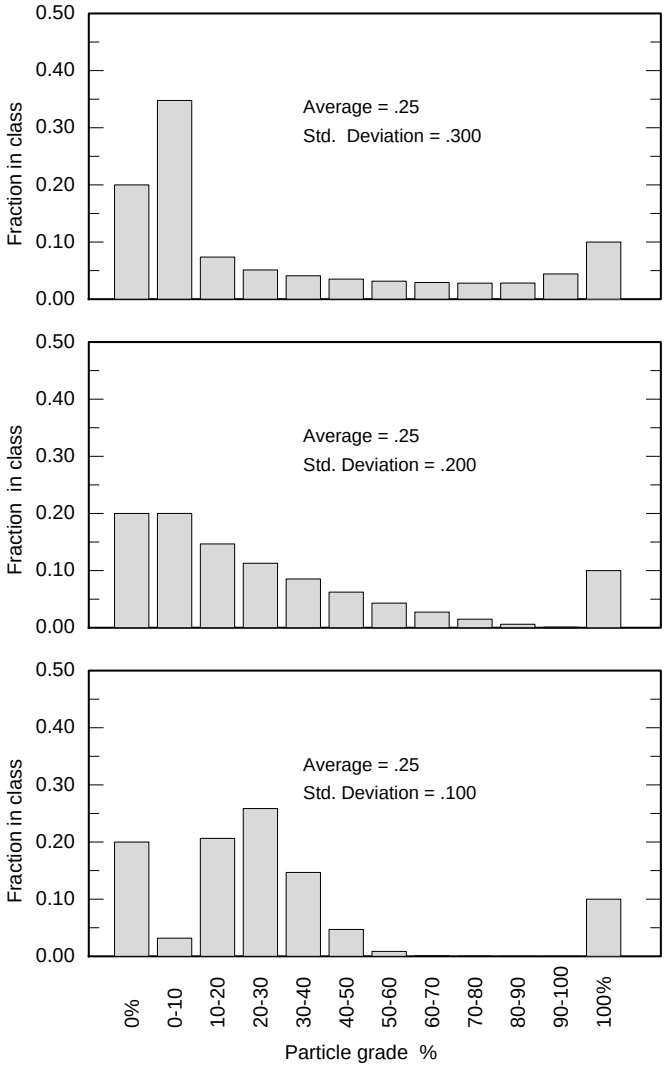


Figure 3.2 The liberation distributions of Figure 3.1 shown as histograms over the grade classes

Although the histogram gives a useful graphical representation of the liberation data, it cannot be used directly to make accurate estimates of the average grade of particles in the population. The usual formula

$$\bar{g} = \sum_{i=1}^{12} g_i p_i(g) \qquad (3.12)$$

will often produce estimates that are significantly in error because of the difficulty in assigning appropriate values to the representative grade $g_i$ of each grade class $i$. An alternative formula which avoids this difficulty is based on the cumulative distribution

$$\bar{g} = \int_0^1 g\,p(g)\,dg = 1 - \int_0^1 P(g)\,dg \qquad (3.13)$$

which is obtained using integration by parts. This integral can be evaluated numerically from a knowledge of the cumulation distribution, *P(g)* at equidistant values of *g*. This can be generated easily from the histogram data as shown in the following example.

Illustrative example 3-1

The histogram data for the distribution shown in the upper graph in Figure 3.2 is given in Table 3.1. Use equations 3.12 and 3.13 to make estimates of the average grade and compare these to the true average.

Table 3.1 Histogram data for the cumulative distribution shown in the top panel of Figure 3.2

| G-class | Grade range | $p_i(g)$ | $P(g)$ | $g_i$ |
|---|---|---|---|---|
| 1 | 0 | 0.2000 | 0.2000 | 0.00 |
| 2 | 0-10 | 0.3478 | 0.5478 | 0.05 |
| 3 | 10-20 | 0.0737 | 0.6215 | 0.15 |
| 4 | 20-30 | 0.0512 | 0.6727 | 0.25 |
| 5 | 30-40 | 0.0410 | 0.7137 | 0.35 |
| 6 | 40-50 | 0.0351 | 0.7488 | 0.45 |
| 7 | 50-60 | 0.0315 | 0.7803 | 0.55 |
| 8 | 60-70 | 0.0292 | 0.8095 | 0.65 |
| 9 | 70-80 | 0.0280 | 0.8375 | 0.75 |
| 10 | 80-90 | 0.0282 | 0.8657 | 0.85 |
| 11 | 90-100 | 0.0343 | 0.9000 | 0.95 |
| 12 | 100 | 0.1000 | 1.0000 | 1.00 |

$$\bar{g} = \sum_{i=1}^{12} g_i p_i(g) = 0.285$$

The integral in equation 3.13 can be conveniently evaluated using any equal-interval quadrature formula such as Simpson's rule rather than the simple Euler formula that is used in equation 3.12 Using Simpson's rule the average grade is calculated to be 0.281. These values can be compared to the correct value of (1 - 0.2 - 0.1)0.25 + 0.1 = 0.275. The error in calculating the average has been reduced from 3.8% to 2.2% using the more accurate formula. The fractional liberation of the two minerals are

$$\mathfrak{L}_1 = 0.275 \times 0.1 = 0.0275$$

and

$$\mathfrak{L}_0 = (1 - 0.275)0.2 = 0.145$$

## 10.3 **Quantitative Prediction of Mineral Liberation**

Minerals are liberated from the host rock of an ore by grinding and in many mineral processing operations the sole purpose of any comminution operation is mineral liberation. Grinding operations are usually unselective in the sense that fractures that are induced in the rock show virtually no correlation with the underlying mineralogical texture of the ore. There are exceptions to this general statement and some of the more important exceptions are examined in some detail later in this chapter. The operations of crushing and grinding can be regarded conceptually as the superimposition of a vast network of fractures through the complex heterogeneous mineralogical texture of the ore. The network of fractures ultimately determines the distribution of particle sizes that are produced in the comminution equipment. The relationship between the network of fractures and the underlying mineralogical texture determines how the mineral phases are distributed among the particles in the population after fracture. This concept can be observed in the particle sections that are shown in Figure 2.9 where the separate mineral phases are displayed at different grey levels so that they can be distinguished easily.

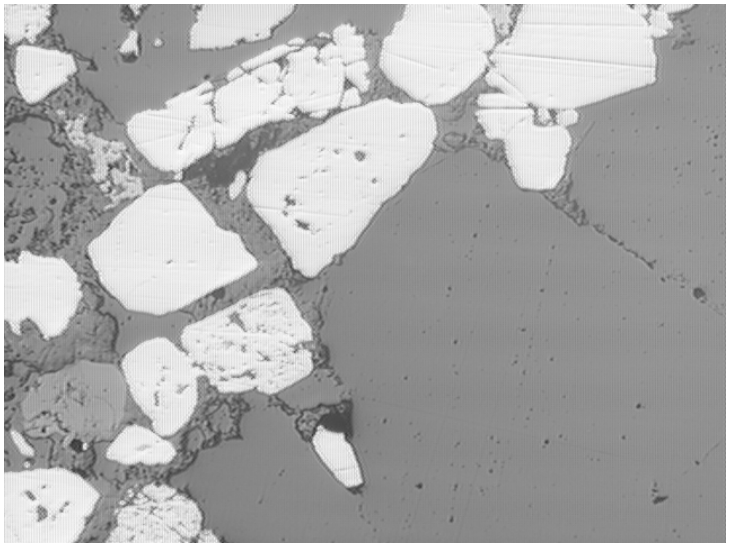

Figure 3.3 Typical image of a section through mineral-bearing ore. Bright phase is pyrite, grey phases are silicates.

The purpose of any mathematical model of the liberation process is the calculation of the liberation distribution that can be expected when mineral ores are subjected to typical comminution operations.

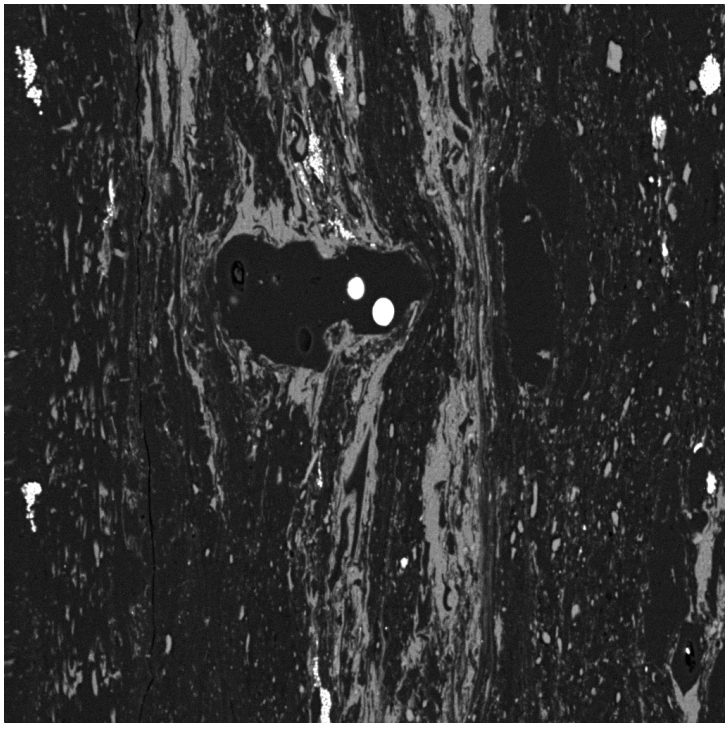

Figure 3.4 Texture of coal. Bright phase is pyrite, grey phase is ash-forming mineral matter and dark phase is the desired carbonaceous material.

Quantitative models that can be used for this purpose are not easy to develop and some specialized methods must be used. Any model for liberation must begin with some quantitative description of the mineralogical texture of the ore. This is no easy task because the ore texture is always complex in the geometrical sense. The most effective tool for the quantitative characterization of texture is image analysis. Samples of the ore are obtained and these are sectioned and polished to reveal a plane section through the material. The section is examined using optical or electron microscopy and many digital images are collected to represent the ore texture. These digital images are analyzed using specialized image analysis software as described in Section 3.3.1. Typical sections through two ores are shown in Figures 3.3 and 3.4.

### 10.3.1 **Characterization of mineralogical texture by image analysis**

Because the texture of ores are so irregular in their geometrical construction it is possible to characterize the texture only in terms of its statistical properties. This requires that many individual observations must be made and the relevant statistical properties of the texture must be estimated from these observations.

The most useful properties to measure are those that will give some measure of the nature of the particles that are formed during grinding. Unfortunately it is not possible to know in advance how any particular piece of ore will fragment during the comminution operations and the fragmentation can only be simulated. The analysis that follows makes use of the concepts of the conditional

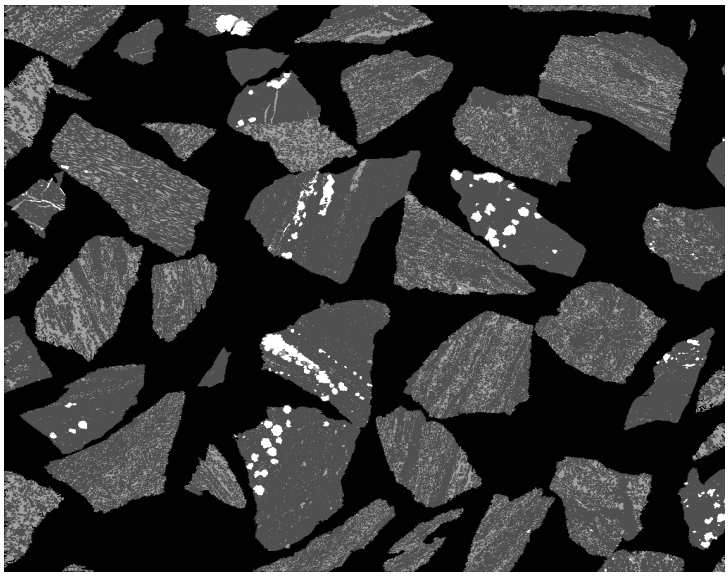

Figure 3.5 Coal particles that were formed by comminution of the texture shown in Figure 3.4

distributions that are discussed in Section 2.6
A simulation of the fracture pattern is obtained from a sample of actual particles which have been mounted, sectioned, polished and imaged as shown for example in Figure 3.5. The size and shape

of these particles are characterized by the distribution of linear intercepts which is determined by measuring the length of very many intercept lengths across the particles as shown in Figure 2.9. This linear intercept pattern, characterizes the particle population and the linear intercept distribution can be used to generate the particle size distribution by solving the integral equation for the mesh size distribution density *p(D)*

$$P(\ell) = \bar{\ell} \int_0^\infty P(\ell|D) \frac{p(D)}{\overline{\ell_D}} dD \tag{3.15}$$

where $\bar{\ell}$ is the average intercept over the whole population and $\overline{\ell_D}$ is the conditional average intercept length for particles that have mesh size *D*. The kernel function $p(\ell|D)$ is the conditional distribution of linear intercept lengths for particles that have mesh size *D*. This kernel function can be measured experimentally but usually only for a sample of particles in a mesh size interval such as the standard $\sqrt{2}$ Series. A function that has been found to be representative of particles that are typically found in the products of comminution operations is

$$\begin{aligned} P(\ell|\Delta D_R) &= 1 - \left(1 - \frac{\ell}{1.2D_{i-1}}\right) \exp\left(-\frac{R^2\ell}{1.2D_{i-1}}\right) \qquad \text{for } \ell \le 1.2D_{i-1} \\ &= 1.0 \qquad\qquad\qquad\qquad\qquad\qquad \text{for } \ell > 1.2D_{i-1} \end{aligned} \tag{3.16}$$

The conditioning variable $\Delta D_R$ indicates that this distribution applies to a sample of particles in a mesh size interval having $\frac{D_{i-1}}{D_i} = R$ rather than at a single size *D*.

When all particles are exactly of size *D*, *R* = 1 and

$$P(\ell|D) = 1 - \left(1 - \frac{\ell}{1.2D}\right) \exp\left(-\frac{\ell}{1.2D}\right) \tag{3.17}$$

It is usual to use distributions that are weighted by length

$$f(\ell) = \frac{\ell p(\ell)}{\bar{\ell}} \tag{3.18}$$

and

$$f(\ell|D) = \frac{\ell p(\ell|D)}{\bar{\ell}_D} \tag{3.19}$$

and equation 3.15 becomes

$$F(\ell) = \int_0^\infty F(\ell|D) p(D) dD \tag{3.20}$$

which has the following useful kernel

$$F(\ell|D) = 1 - \exp\left(-\left(\frac{\ell}{0.772D}\right)^{\lambda}\right) \tag{3.21}$$

where the parameter $\lambda$ is a function of the material and method of comminution.

The distributions given in equations 3.16 and 3.17 are parameter free and can be used for many ores even when the linear intercept distribution for the particles is not available. When the conditional linear intercept distribution of the particle population is known or can be estimated, the prediction of the expected liberation characteristics of the ore can be calculated using the following straightforward method.

The image of the unbroken ore is sampled by superimposing linear samples drawn from the population defined by equation 3.15. Each linear sample will cover one or more of the phases and consequently can be characterized by its linear grade $g_L$ which is the fraction of its length that covers the mineral phase. The sample lengths can be sorted into sizes and the distribution of linear grades can be easily estimated for each different linear sample length which generates the conditional linear grade distribution $P(g_L|\ell)$ for the ore. This provides the necessary characterization of the ore texture from which its liberation characteristics can be calculated.

The images that are used must be larger than the largest dimension of any texture characteristic of the ore. This can be difficult to achieve if the size scales of the different minerals in the ore are widely different. The pyritic quartzite and coal shown in Figures 3.3 and 3.4 are typical examples. The pyritic quartzite includes large quartz pebbles which are completely barren and the dimensions of the carbonaceous phase in coal are very much larger than the pyrite and ash grains. The images must be collected at sufficiently high resolution to capture all of the essential features of the texture of the finest mineral grains and at the same time they must reveal the full texture of the largest mineral grains. Generally this is not possible in a single image since the field of view of any microscope is limited. This problem can usually be overcome by collecting images that are contiguous and then stitching these together to form a single long image from the sequence of smaller images. The linear sample lines can be sufficiently long to cover the largest feature in the texture while the full resolution of the original image is maintained. An example formed by stitching the pyritic quartzite images is shown in Figure 3.6.

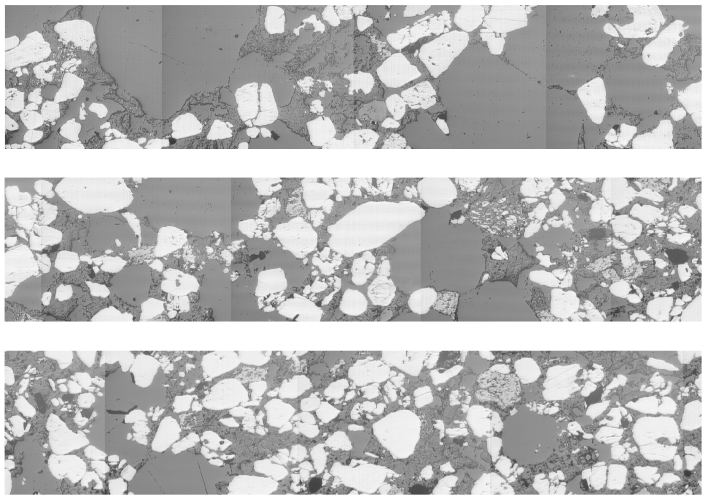

Figure 3.6 Stitched images of unbroken pyritic quartzite ore. Slight grey-level differences between contiguous images have been introduced to reveal where images have been stitched. Images were collected using optical microscopy at 2.5µm per pixel and each strip shown is 2328 x 480 pixels.

The three strips shown in Figure 3.6 actually formed one single strip for analysis and the longest linear sample that covered only one phase was found to be 1042 pixels in this sample. Normally about five strips of stitched images are analyzed to characterize a single polished section and many polished sections are collected to ensure that the ore is adequately sampled. The linear sampling lines are laid down on the image in a head-to-tail pattern to ensure that each portion of the texture is sampled only once since no point in the original ore texture can appear in more than one particle after comminution.

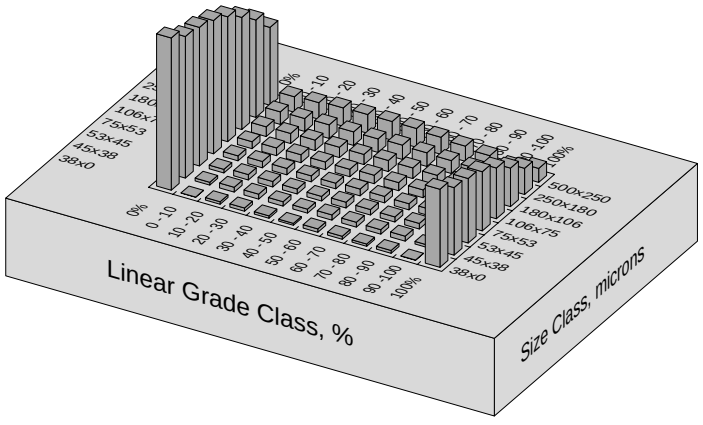


Figure 3.7 Calculated distribution of linear intercepts as a function of particle size for the texture shown in Figure 3.6.

The liberation distribution that can be expected when this ore is comminuted can be calculated using the following two-step procedure. In the first step the measured distribution of linear grades from the linear samples are combined with the linear intercept distribution density $p(\ell|D)$ of the particles that are expected to be formed during comminution of the ore. Equations 3.16, 3.17 or 3.21 would be suitable models for the latter distribution. This produces the distribution of linear grades in particles of size $D$ from the equation

$$P(g_L|D) = \int_0^\infty P(g_L|\ell)\,p(\ell|D)\,d\ell \qquad (3.22)$$

This equation represents exactly the measurement of the linear grade distribution by sampling particle sections from size $D$ as described in Section 2.7.2. The result of applying this transformation to the distribution of linear grades measured on the texture shown in Figure 3.6 is given in Figure 3.7.

Equation 3.22 implies that $P(g_L|\ell,D)$ is independent of the particle size. This is valid provided that the fracture process is random and independent of the texture. The problem is considerably more complex when non-random fracture patterns occur. Non-random fracture is discussed in Section 3.5

In the second stage of the calculation, the distribution of linear grades that was calculated using equation 3.22 is transformed stereologically to generate the distribution of grades in the real three dimensional particles. This is identical to the problem discussed in Section 2.7.3 for stereologically transforming measured linear grade distributions. The solution method is based on generating solutions to the integral equation

$$P(g_L|D) = \int_0^\infty P(g_L|g,D)\,p(g|D)\,dg \qquad (3.23)$$

Unlike equation 3.22, equation 3.23 cannot be solved in a straightforward manner because the required solution is the function $p(g|D)$ that appears under the integral in the right hand side. However, appropriate solution methods are available and the solution can be generated easily using a number of computer software packages that are readily available as discussed in Section 2.7.2 The result of applying the stereological transformation to the data shown in Figure 3.7 is given in Figure 3.8. The difference in the "liberation sizes" of the pyrite and silicates is clearly evident. Liberated silica particles can be as large as 250 µm

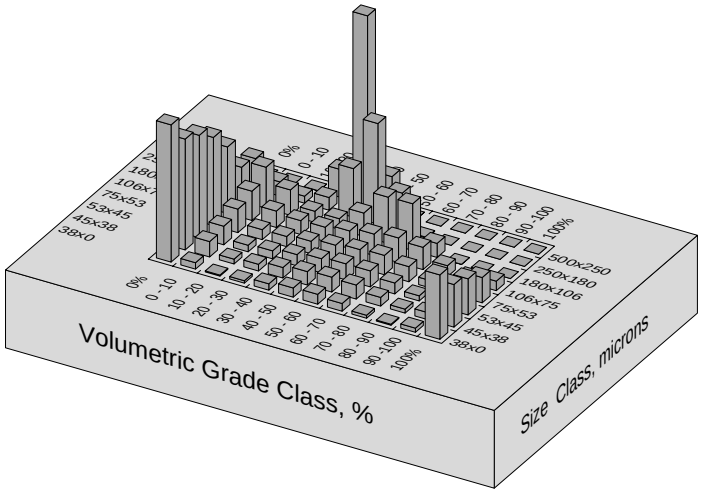


Figure 3.8 Data of Figure 3.7 after stereological transformation to calculate the predicted liberation as a function of particle size after comminution.

while the largest liberated pyrite particle is no larger than 106 µm.

## 10.4 **Simulating Mineral Liberation During Comminution**

### 10.4.1 **Boundaries of the Andrews-Mika diagram.**

The method that was described in Section 3.3 can be used to predict the liberation distribution that will result when an ore is broken in a random fashion and no other processes are involved that will change the make-up of the particle population. Processes such as classification and concentration can have a large effect on the relative distribution of particle types. In particular there must be no preferential selection of particle types during the entire comminution process. These conditions are normally not met in ball mill circuits which usually process feed that includes cyclone underflow and often other concentrates and tailing streams in addition to fresh feed. This complicates the calculation of the mineral liberation during comminution and it is necessary to apply population balance techniques which can describe the fracture of multi-component particles on a class-by-class basis. In this way the grade classes can be accurately accounted for among the breaking particles and evolution of the liberation distribution can be calculated at all stages in the comminution process.

The effect of the mineral liberation phenomenon is described in the population balance models through the breakage matrix $b(\boldsymbol{x};\boldsymbol{x}')$ in equation 2.117. This matrix describes how particles transfer among the internal coordinates during comminution. Two internal coordinates, particle size and particle grade, are required to describe populations of multi-component particles. The matrix $b(\boldsymbol{x};\boldsymbol{x}')$ is difficult to model in any particular case because it depends on both the liberation characteristics of the material, which are governed primarily by mineralogical texture, and also by the characteristics of the comminution machine. In spite of the complexities, useful models have

been developed and these have proved to be successful in simulations of complex milling and concentration circuits. The approach that is used here is based on a graphical representation of the breakage process called the Andrews-Mika diagram. These diagrams show what type of progeny particles will be generated when a single parent particle breaks in a milling environment. The diagrams are useful because the graphical representation is fairly easy to interpret and the diagrams explicitly include a number of essential constraints that must be applied to the breakage process in the population balance modeling method.

Particle size and particle grade must be included among the internal coordinates to describe mineral liberation and the vector $\boldsymbol{x}$ of internal coordinates is written for a two-component ore as

$$\boldsymbol{x} = (g, d_p) \tag{3.24}$$

Here $d_p$ represents the particle size and $g$ the particle grade. The breakage matrix $b(\boldsymbol{x};\boldsymbol{x}')$ can be written as

$$b(\boldsymbol{x};\boldsymbol{x}') = b(g, d_p; g', d_p') \tag{3.25}$$

to reflect the two variables that make up the internal coordinates. This function can be simplified significantly using the rules of conditional distributions discussed in Section 2.6

$$b(g, d_p; g', d_p') = b(g \mid d_p; g', d_p')\, b(d_p; g', d_p') \tag{3.26}$$

To a large extent this decouples the breakage process from the liberation process and the two breakage functions can be modeled separately and then subsequently combined using equation 3.26 to generate the transformation function $b(g,d_p;g',d_p')$ which is necessary to apply the population balance method. The function $b(d_p;g',d_p')$ can, in most cases, be assumed to be independent of the grade $g'$ of the parent particle.

$$b(d_p; g', d_p') = b(d_p; d_p') \tag{3.27}$$

This is equivalent to asserting that the breakage function is independent of the grade of the parent particle. This appears to be a realistic assumption in most practical cases. Models for the breakage function $b(d_p;d_p')$ are discussed in Section 5.4. The function $b(g \mid d_p; g', d_p')$ shows how the fracture products of a parent particle of size $d_p'$ and grade $g'$ are distributed with respect to grade for every possible progeny size. A useful practical model for this function is developed in this section.

A geometric approach is taken and the nature of the function is described by reference to the two-dimensional $g - d_p$ plane as shown in Figure 3.9 Any particle is located in this plane according to

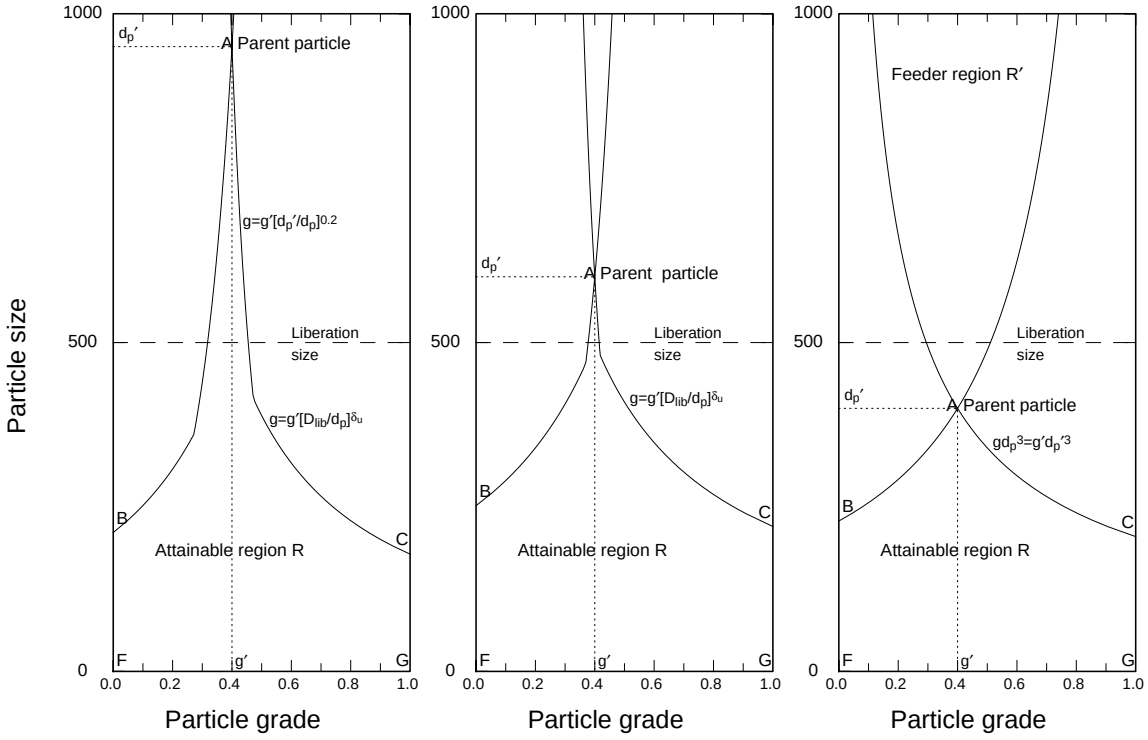


Figure 3.9 Boundaries of the Andrews-Mika diagram for the three cases: parent particle size > liberation size, parent particle size ≈ liberation size and parent particle size < liberation size.

the values of its mineral grade $g$ and its size $d_p$. We wish to investigate how the progeny particles of a single parent will dispose themselves in this two-dimensional phase space after breakage when the location of the parent particle is known. Of course this can be determined only in a probabilistic sense because the fracture process is random in character. Thus the liberation distributions for progeny particles from a parent at point $g'$, $d_p'$ is required. To use the simplification that is inherent in equation 3.26, the distributions that are conditional on the progeny size, $d_p$, are calculated. This gives the function $b(g|d_p;g',d_p')$ which can be combined with the breakage function $b(d_p;d_p')$ in equation 3.27 for use in the population balance equation 2.117. A geometrical model is developed here for $b(g|d_p;g',d_p')$ in terms of a comparatively small number of parameters that can be related to features of the mineralogical texture of the parent particle.

Consider a parent particle at point A in Figure 3.9. When this particle is broken, the progeny particles cannot appear at every point in the phase space. They are restricted by definite physical constraints. Clearly progeny can appear only below point A because every progeny particle must be smaller than the parent. In addition the progeny particles must satisfy the law of conservation of phase volume. This means that no progeny particle can contain a greater volume of mineral than the volume of

mineral in the parent particle. Likewise no progeny particle can contain more gangue than was present in the parent particle. These restrictions lead to the two inequalities

$$g v_p \leq g' v_p' \tag{3.28}$$

and

$$(1 - g) v_p \leq (1 - g') v_p' \tag{3.29}$$

where $v_p$ is the volume of the progeny particle and $v_p'$ the volume of the parent particle. Since particles that are produced during comminution are more or less geometrically similar, these inequalities can be written approximately as

$$g d_p^3 \leq g' d_p'^3 \tag{3.30}$$

and

$$(1 - g) d_p^3 \leq (1 - g') d_p'^3 \tag{3.31}$$

These inequalities define two regions R and R′ in the phase space like those shown in the right hand panel of Figure 3.9 The diagrams shown in Figure 3.9 are called Andrews-Mika diagrams in recognition of the first paper that described the boundaries and explored their significance.

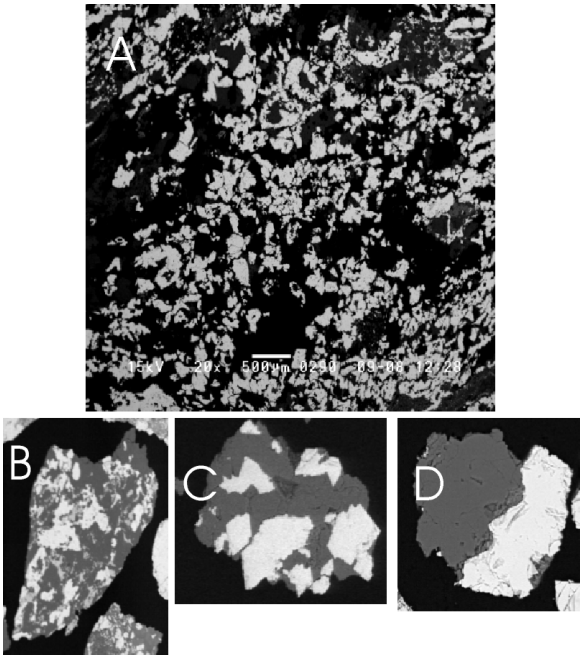


Figure 3.10 Images that show the non-fractal nature of a typical mineralogical texture. A is a section through the unbroken ore. B is a section through a single particle from the 950-1180 µm screen fraction at 20× magnification. C is from the 212-300 $\mu$m screen fraction at 70× magnification. D is from the 53-75 $\mu$m screen fraction at 300× magnification.

The region R, called the attainable region, shows where progeny particles can appear after fracture of a parent at point A. In particular the liberated edges of the region, represented by BF and CG in the diagram, are included in the attainable region because an unliberated particle can generate completely liberated particles. However, it is physically impossible for a parent at A to generate any liberated particles larger than $d_{pC}$ or liberated gangue particles larger than $d_{pB}$. The region R′ is complementary to R and represents the region of phase space that contains parent particles that could produce a progeny at point A. This region is called the feeder region for progeny at A. Unlike the attainable region, the boundaries of the feeder region neither intersect nor touch the vertical sides of the diagram at $g = 0$ and $g = 1$ because of the obvious fact that an unliberated progeny can never be produced from a liberated parent. The feeder region is important because it appears in the fundamental population balance equation 2.111 for comminution machines and it is necessary to establish the boundaries of R′ to define the region of integration in that equation. The shape of the boundaries of R and R′ vary considerably depending on the location of the parent particle in the phase space.

When the parent particle is significantly smaller than the average "grain size" of the mineral in the ore, the parent will appear under the microscope as shown in image D of Figure 3.10. Under these conditions the parent will typically contain only a single region of mineral and a single region of gangue and inequalities 3.30 and 3.31 are realistic bounds for the regions R and R′.

This is not true when the parent particle is significantly larger than the mineral "grain size". Two other cases can be distinguished: the parent size is comparable to the mineral "grain size" and the situation when the parent size is much larger than the mineral "grain size". These situations are illustrated in images B and C respectively Figure 3.10 which are from the same material but were made from particles of different size and magnification. The texture appears to change from size to size but it is only the apparent texture that changes. The overall texture is of course the same. Textures that display this characteristic are called non-fractal to distinguish them from synthetic textures made using fractal generators and which appear to be qualitatively similar no matter what scale and magnification is used to observe them. If the texture were truly fractal, each apparently uniform mineral grain in Figure 3.10 would appear to be fragmented and made up of much smaller grains.

These geometrical properties of textures affect the boundaries of the feeder and attainable regions. This can be seen most easily by considering point C in the right hand panel of Figure 3.9 which is drawn at the intersection of the boundary of the attainable region and the line $g = 1$. This point reflects the principle that the largest completely liberated progeny particle cannot exceed the total size of the mineral phase in the parent. If the parent particle contains only a single mineral grain as is suggested, for example, by the lower image in Figure 3.11, the largest grain is proportional to $g' d_p'^3$ which is reflected in inequality 3.30. However, when the parent particle contains several separate mineral grains as shown in the upper diagram in Figure 3.11, the intersection of the attainable region boundary with $g = 1$ must reflect the principle that the size of the largest liberated mineral particle in the progeny population cannot exceed the size of the largest single coherent mineral grain in the parent particle. If there is more than one grain in the parent the size of the

largest single grain must be smaller than $g' d_p'^3$ and the upper boundary of the attainable region must fall below $g' d_p'^3$. This is illustrated in the left hand and center panels of Figure 3.9. Similar arguments can be made for the gangue phase, which is reflected in the left hand boundaries of the attainable regions shown in Figure 3.9 Boundaries for the feeder and attainable regions for this situation can be defined by analogy to inequalities 3.30 and 3.31 as

$$\begin{aligned} g d_p^{\delta} &\le g' d_p'^{\delta} \\ (1-g) d_p^{\delta} &\le (1-g') d_p'^{\delta} \end{aligned} \tag{3.32}$$

with $\delta \le 3$. The exponent $\delta$ varies with parent size and a model for this variation that has been found to be useful in practice is

$$\delta = \min\left[ \delta_0 \left( \frac{D_{lib}}{d_p'} \right)^x, 3 \right] \tag{3.33}$$

for $d_p' \le D_{lib}$ where $D_{lib}$ is a parameter referred to as the liberation size for the ore. It is roughly equal to the particle size at which the mineral starts to liberate significantly when the ore is comminuted. $X$ is a parameter which is approximately 0.5. The upper limit of $\delta = 3$ represents the law of conservation of phase volume and must never be exceeded.

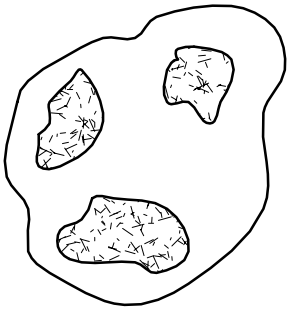

Conservation of total volume
Volume of the largest liberated mineral progeny particle cannot exceed the total volume of all mineral grains in the parent particle.

Conservation of grain volumes
The volume of the largest liberated mineral particle cannot exceed the volume of the largest single mineral grain in the parent particle

When the parent particle is much larger than the mineral grain size, the boundaries of the Andrews-Mika diagram are controled by the grain volume constraint.

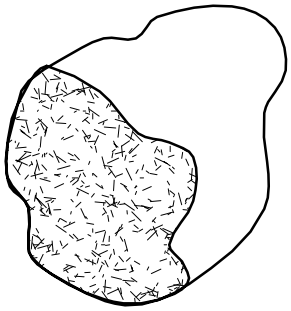

Volume of a single grain of mineral in the parent is the same as the total volume of mineral.

When the parent particle is much smaller than the mineral grain size, both conservation principles give the same limit for the maximum liberated particle size.

Figure 3.11 Images showing the non-fractal nature of mineralogical textures.

The symmetry of the texture is also an important factor in fixing the boundaries of the attainable and feeder regions. A symmetrical texture is one in which the different mineral phases cannot be distinguished from geometrical factors alone. The most common asymmetric texture is one in which distinct grains of one mineral are imbedded in a more or less continuous phase of another mineral. To account for this effect the exponent $\delta$ can be different for the mineral and the gangue. Thus inequalities 3.30 and 3.31 are written

$$\begin{aligned} g\, d_p^{\delta_u} &\le g' d_p'^{\delta_u} \\ (1-g) d_p^{\delta_l} &\le (1-g') d_p'^{\delta_l} \end{aligned} \tag{3.34}$$

The asymmetry factor for the texture is the ratio $\delta_u/\delta_l$ with $\delta_u \delta_l = \delta$.

When the parent size is much greater than the liberation size $D_{lib}$, and when the progeny particles are also larger than $D_{lib}$, these will retain the parent composition or at most will be only slightly less or slightly greater than the parent composition. The attainable region is narrow for these progeny and useful approximations to the boundaries are shown in the left hand panel of Figures 3.9 and are

given by

$$g_u \leq \max\left[g'\left(\frac{d_p'}{d_p}\right)^{0.2},\ g'\left(\frac{D_{lib}}{d_p}\right)^{\delta_u}\right] \tag{3.35}$$

$$1 - g_l \leq \max\left[(1-g')\left(\frac{d_p'}{d_p}\right)^{0.2},\ (1-g')\left(\frac{D_{lib}}{d_p}\right)^{\delta_l}\right] \tag{3.36}$$

In spite of the empirical nature of these relationships, the parameters can be estimated reliably from batch comminution tests on two-component ores.

### 10.4.2 **Internal structure of the Andrews-Mika diagram**

The boundaries of the Andrews-Mika diagram are not sufficient to define how progeny particles are distributed when a parent of given size and grade is broken. The internal structure of the diagram contains this information and a useful model for this internal structure is developed here which is

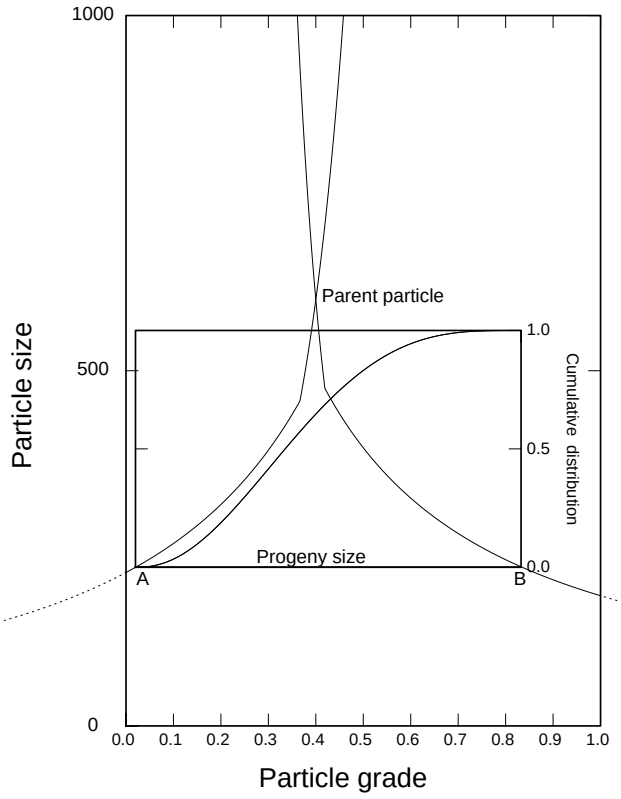


Figure 3.12 Use of the Beta distribution to model the internal structure of the Andrews-Mika diagram when neither mineral is liberated.

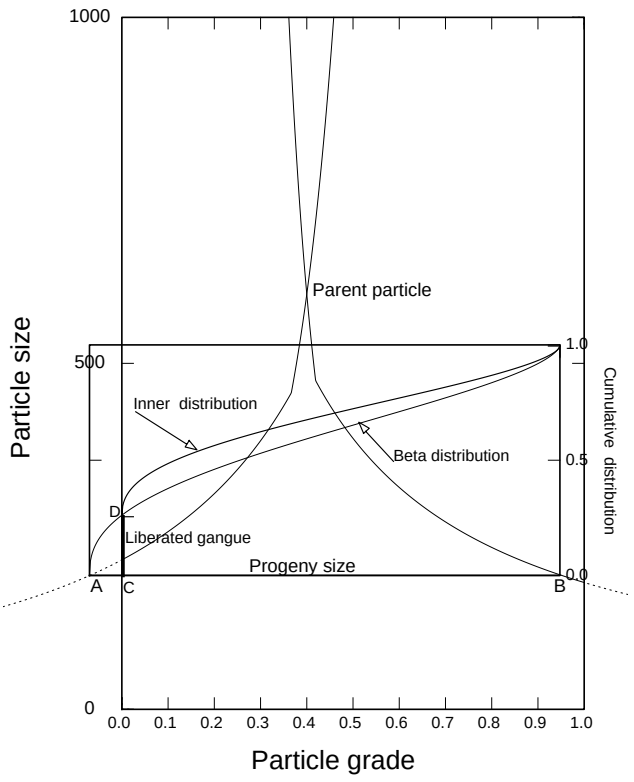


Figure 3.13 Use of the Beta distribution to model the internal structure of the Andrews-Mika diagram when the gangue phase is liberated but the mineral is not liberated.

based on the Beta distribution.

The model is based on the assumption that the progeny particle population at any size will have a Beta distribution with respect to particle grade. For progeny having size not much less than the parent, the distribution will be bell-shaped around the parent particle grade and as the progeny size gets further below the parent size, the particles show successively more liberation and the distribution exhibits the characteristic U-shape with more and more particles appearing at or near the liberated ends of the distribution. The Beta distribution provides a good model for this type of behavior and the change from bell-shaped to U-shaped distribution is modeled by a steadily increasing variance as the progeny size decreases.

The Beta distribution itself does not account for completely liberated material at g = 0 and g = 1. At any horizontal level in the Andrews-Mika diagram where the boundaries of the attainable region are inside the limits $g = 0$ and $g = 1$ as shown for example by line A-B in Figure 3.12 there are no liberated particles and the total distribution is given by the inner Beta distribution alone which extends from A to B. At progeny particle sizes where at least one of the boundaries of the attainable region is a vertical edge at g = 0 or g = 1, liberated particles are present in the population. It is necessary to calculate what fraction of the particle population appears as liberated particles at grades $g = 0$ and $g = 1$.

A method to accomplish this is based on the following construction. The curved boundaries of the attainable region are extended out past $g = 0$ and $g = 1$ as shown by the broken lines in Figures 3.13 and 3.14 At any progeny size, the grade distribution is assumed to be beta distributed from one extended boundary to the other but the distribution is truncated at $g = 0$ and $g = 1$ with all the probability mass in the distribution from $g = g_l$ (point A) to $g = 0$ concentrated at $g = 0$ and all the probability mass in the distribution from $g = 1$ to $g = g_u$ (point B) concentrated at $g = 1$. This represents the liberated gangue and liberated mineral respectively. The liberated gangue, $L_0$, is given by the length of the line CD in Figures 3.13 and 3.14. The liberated mineral is given by the length of the line FE in Figure 3.14 The remainder of the particle population is then distributed internally as a Beta distribution as described in Section 3.1 There is an upper limit to the amount of liberated mineral or liberated gangue in the particle population. This is clearly the amount of mineral or gangue respectively in the original

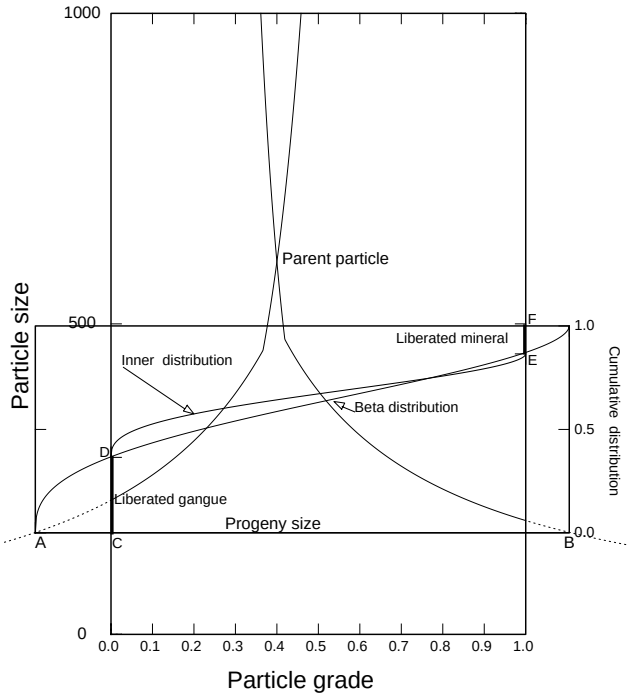


Figure 3.14 Use of the Beta distribution to model the internal structure of the Andrews-Mika diagram when the both gangue phase and the mineral phase are liberated.

parent particle. If the construction described above produces a value larger than either of these it is assumed that the liberation is complete and that the internal distribution is empty.

The internal distribution will not extend over the entire range from $g = 0$ to $g = 1$ if one or both of the boundaries are inside this range at the progeny size in question as shown for example in Figures 3.12 and 3.13. This situation is handled by noting that the transformed variable

$$\chi(g) = \frac{g - g_l}{g_u - g_l} \tag{3.37}$$

has a Beta distribution over the $\chi = 0$ to $\chi = 1.0$ with variance $\sigma^2$.

The variance of the conditional grade distribution also increases as the progeny size decreases reflecting the greater tendency for liberation as the progeny becomes smaller. The internal distribution changes from bell-shaped to U-shaped as the variance increases.

The variance of the distribution is also influenced by the parent grade. When the parent particle has a grade close to 0.5, the grades of the progeny can spread more easily over the range $g = 0$ to $g = 1$ than when the parent particle is closer to either end of the grade scale. The variation in variance of the progeny distribution with respect to both parent grade and progeny size is given by

$$\sigma^2 = g'(1 - g')f(d_p) \tag{3.38}$$

with

$$f(d_p) = \frac{1}{1 + \left(\frac{d_p}{D_{lib}}\right)^{\lambda}} \tag{3.39}$$

The function $f(d_p)$ is S-shape in the range 0 to 1 as $d_p$ varies from large sizes to very small sizes. This function has the greatest variation when $d_p$ is close to the mineral liberation size which reflects the tendency of the mineral to liberate over a comparatively narrow range of sizes. This phenomenon has often been observed in typical ore textures.

Substitution of equation 3.38 into equation 3.7 gives

$$\gamma = \frac{1 - f(d_p)}{f(d_p)} \tag{3.40}$$

The parameters of the internal distribution must be chosen so that the average grade of the conditional distribution at every progeny size is equal to the parent grade

$$\overline{g}^M = \int_{g_l}^{g_u} g\,p(g|d_p;g',d_p')\,dg = \frac{g' - L_1}{1 - L_1 - L_0} \tag{3.41}$$

The two parameters of the internal distribution are calculated from $\alpha^M = \overline{g}^M\gamma$ and $\beta^M = (1 - \overline{g}^M)\gamma$. In fact, equation 3.41 holds only if the fracture process is random and no preferential breakage of one or other of the mineral phases occurs. Preferential breakage is discussed in Section 3.5

## 10.5 **Non-Random Fracture**

When the fracture pattern that is developed in the ore during comminution is not independent of the mineralogical texture, the fracture process is considered to be non-random. Significant progress has been made during the past decade on quantifying the effects of nonrandom fracture when particle fracture is influenced by the mineralogical composition and the texture of the parent particle. Six separate nonrandom fracture effects have been identified when multi phase particles are broken.

1. *Selective breakage.* This occurs when the different mineral phases have unequal brittleness. The more brittle mineral fractures more easily, and accordingly particles that have a larger content of the more brittle phase will have a larger specific rate of breakage. This phenomenon does not influence the nature of the Andrews-Mika diagram directly and is described entirely through the breakage rate parameters in the population balance equation. The parameter *k* in equation 5.74 must be considered to be a function of both the particle size and the grade of the particle. This is discussed further in Section 5.8.3

2. *Differential breakage.* This occurs when the conventional breakage or appearance function depends on the composition of the parent particle. In other words, the size distribution of the progeny from a single breakage event will be influenced by the composition of the parent particle.

3. *Preferential breakage.* This occurs when crack branching occurs more frequently in one of the mineral phases. The most obvious manifestation of preferential breakage is a variation of average composition with particle size in the particle populations. This is often noticed in practice and is usually comparatively easy to detect and measure. Good models are available to incorporate preferential fracture into the Andrews-Mika diagram and comparisons with experimental observations have been satisfactory.

4. *Phase-boundary fracture.* This occurs when cracks have a significant tendency to move along interphase boundaries rather than across the phases. Phase-boundary fracture destroys interphase boundary area in the progeny particles, and this should be measurable by careful image analysis. However, no convincing evidence of significant phase-boundary fracture has been reported in the literature.

5. *Liberation by detachment.* This occurs when mineral grains are comparatively loosely bonded into the ore matrix. Mineral grains become detached from the ore during comminution, which leads

to significant and clean liberation of the mineral phases. This is unfortunately a fairly rare phenomenon and is not often encountered with large ore bodies.

6. *Boundary-region fracture*. This occurs when the highly stressed region in the neighborhood of the boundary between two dissimilar minerals is preferentially fractured. This leads to the production of comparatively more smaller particles from the phase boundary region and therefore to less liberation among finer particles than among coarser particles which originate preferentially from the interior of the mineral phases. Although there is some direct evidence that boundary-region fracture does occur, this phenomenon is usually inferred from indirect observations on the behavior of the particles in concentration plants. For example, preferential fracture in the neighborhood of a minor mineral component will lead to a more than proportionate showing of that mineral on the surfaces of the particles. This can have a profound effect on the response of the particles to flotation. This is a complex phenomenon and no quantitative models have yet been developed to describe the effect convincingly.

Only the first three of these six non-random fracture effects have been modeled successfully and the last three require considerably more research. Selective breakage can be simulated by determining the brittleness of each mineral species and modeling the selection function in terms of the brittleness ratio ß as follows

$$k_0(g,d_p) = \frac{2(g + (1-g)ß)\, k_0(d_p)}{1 + ß} \tag{3.42}$$

In equation 3.42, $k_0(d_p)$ is the specific rate of breakage as a function only of the size of the parent particle. Models for $k_0(d_p)$ are discussed in Section 5.12. The brittleness ratio can be measured using micro indentation techniques on polished sections of the minerals.

When differential breakage occurs the approximation of equation 3.27 cannot be used and the size breakage function and a collection of breakage functions for each parent composition must be used. Such breakage functions can be measured in the laboratory using single impact or slow compression testing devices.

If one of the mineral phases breaks preferentially it will end up in greater concentration in the finer sizes after comminution. Although it is not possible to predict this phenomenon from a study of the mineralogy, it can be observed easily in size-by-size assays of a simple laboratory batch mill test. This will reveal the systematic variation of mineral content with size. Preferential breakage has a strong influence on the internal structure of the Andrews-Mika diagram. Equation 3.41 can be relaxed and replaced with the requirement that the average mineral grade over the total particle population must be conserved. Thus

$$\int_0^{d_p'} \int_0^1 g\, b(g, d_p | g', d_p')\, dg\, dd_p = g' \tag{3.43}$$

for every combination of parent grade and size. Using equation 3.26 this restriction becomes

$$\int_0^{d_p'} b(d_p | g', d_p') \int_0^1 g\, b(g | d_p; g', d_p')\, dg\, dd_p = g' \tag{3.44}$$

The preferential breakage is modeled by finding how the conditional mean

$$\bar{g}(d_p; g', d_p') = \int_0^1 g\, b(g | d_p; g', d_p')\, dg \tag{3.45}$$

of the progeny particles varies with their size and parent composition. A model that has been found to satisfy data for several ores is

$$\bar{g}(d_p; g', dp') = g' \pm \phi g'(1 - g') v\left(\frac{d_p}{d_p'}\right) \tag{3.46}$$

with

$$\int_0^{dp'} b(d_p | g', d_p')\, v\left(\frac{d_p}{d_p'}\right) dd_p = 0 \tag{3.47}$$

Provided that the function $v\left(\frac{d_p}{d_p}\right)$ satisfies equation 3.47, the conservation constraint will be satisfied. The positive sign is used in equation 3.46 when the mineral fractures preferentially and the negative sign is used when the gangue fractures preferentially.

A function which satisfies this requirement and which is suggested by typical experimental data is

$$v(u) = u^{\alpha} \ln(u) \tag{3.48}$$

with

$$\alpha = -\frac{1}{\ln(u*)}$$

$$u = \frac{1 - \frac{d_p}{d_p'}}{1 - \Delta_0} \tag{3.50}$$

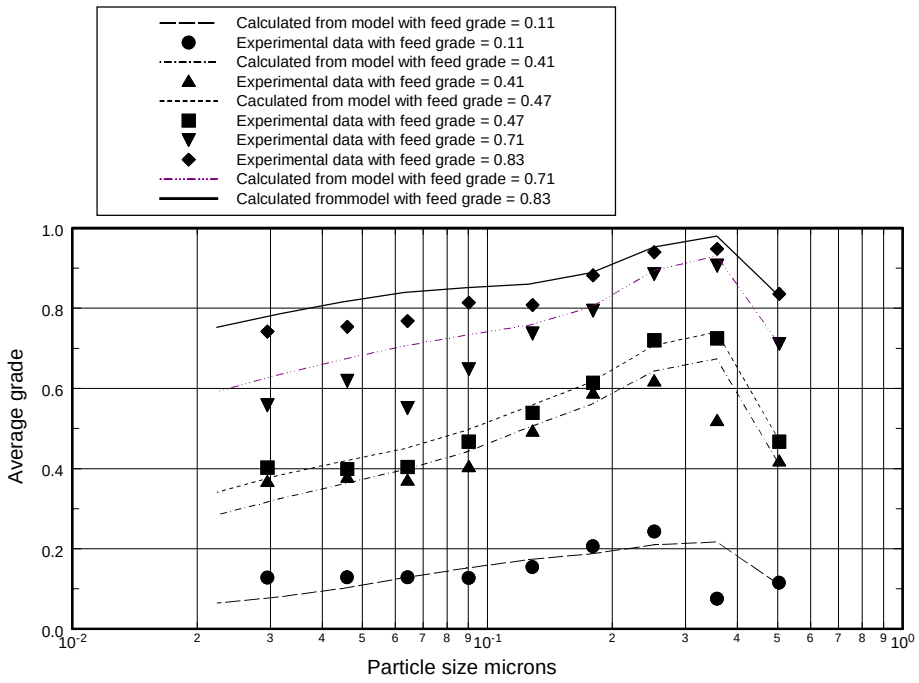


Figure 3.15 Data showing variation of grade with particle size when preferential breakage occurs.

This model for preferential breakage has two parameters. Values for these parameters must be found from experimental data. $\Delta_0$ is a parameter that is adjusted to satisfy equation 3.47. $u^*$ can be estimated directly from a plot of mineral grade against particle size in the comminution product. Usually such a plot shows a clear maximum or minimum. $u^*$ is the value of $u$ at the maximum or minimum. The data shown in Figure 3.15 demonstrates this.

## 10.6 **Discretized Andrews-Mika diagram**

The models for the boundaries and internal structure of the Andrews-Mika diagram that are developed in the preceding sections are based on the continuous Beta distribution. They are particularly useful for calculations in this form and discrete versions are developed here for use in the discretized population balance models for ball mills that are described in Chapter 5. It is common practice to classify the grade variable into 12 or 22 classes over the range [0,1]. 12 classes allow one class at each end of the distribution for liberated mineral and for liberated gangue and 10 intervals in (0,1). These are often of equal width but this is not essential. 22 classes allow for 20 internal classes which are usually 0.05 grade units in width. The conditional discrete distribution can be obtained from the cumulative conditional distribution using the following equations

$$\begin{aligned} p_i(g_i|d_{pj};g_k',d_{pl}') &= P(G_{i+1}|d_{pj};g_k',d_{pl}') - P(G_i|d_{pj};g_k',d_{pl}') \\ &= (1-L_0-L_1)\left(I_{\xi(G_{i+1})}(\alpha^M,\beta^M) - I_{\xi(G_i)}(\alpha^M,\beta^M)\right) \end{aligned} \tag{3.51}$$

$G_i$ is the grade at the boundary between the *i-1* and *i* grade class.

A shorthand notation is used to describe the discrete versions of these distribution functions.

$$a_{i,jkl} = p_i(g_i|d_{pj};g_k',d_{pl}') \tag{3.52}$$

The coefficients $a_{i,j,k,l}$ make up a discrete version of the attainable region of the Andrews-Mika diagram and an examples are shown in Figures 3.16 and 3.17. Each bar in the attainable region shows what fraction of the parent particle transfers to each progeny class on breakage. The bar heights in the diagram are normalized so that the total height of all bars at a particular size is unity. This is consistent with the use of the conditional distributions in the continuous models described in Sections 3.4 and 3.5.

When this model for mineral liberation is inserted into the population balance equations for the ball mill, the feeder region for each point in the phase space rather than the attainable region from each parent location is required. The models developed in Sections 3.4 and 3.5 provide a logical and consistent description of the attainable region and it would be much more difficult to develop models for the feeder region. It is simpler to generate the feeder region from the known structure of the attainable region. Let $b_{i,jkl}$ be the fraction of size *l* to size *j* transfers that appear in grade class *i* when the parent is in grade class *k*. The relationship between the attainable and feeder regions is

$$b_{i,jkl} = a_{k,jil} \tag{3.53}$$

Thus to construct a complete feeder region for any progeny particle, a complete set of attainable regions must be available for all possible parents.

Typical examples of the discretized Andrews-Mika diagram are shown in Figures 3.16 and 3.17. It is important to realize that these represent just two of the many discrete Andrews-Mika diagrams that are required to characterize any particular ore. Figures 3.16 and 3.17 show a discretization over 19

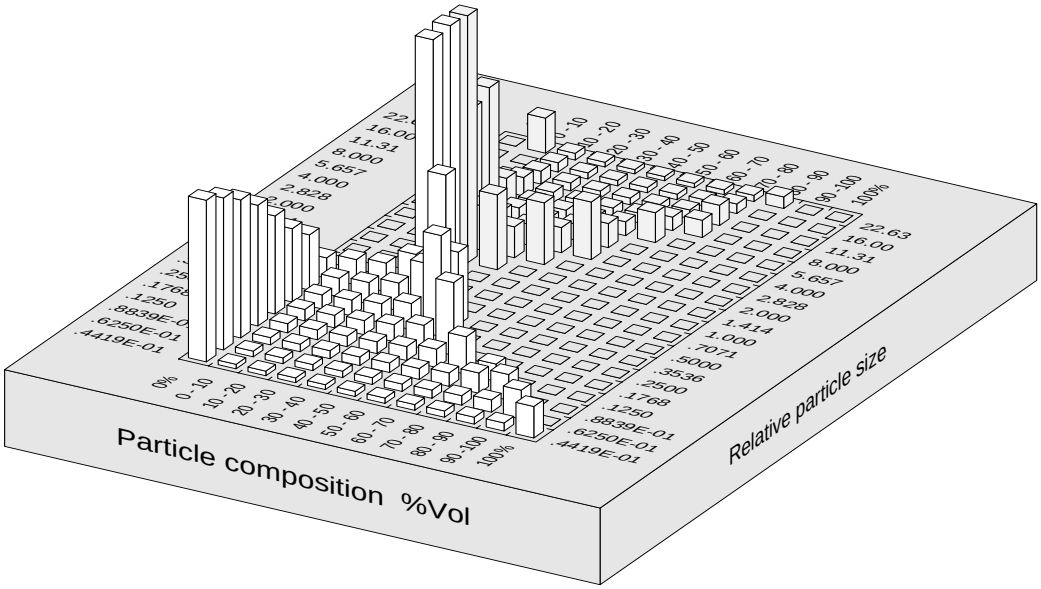


Figure 3.16 Internal structure of a typical Andrews-Mika diagram showing both the feeder and attainable regions. The feeder region is indicated by the shaded bars in the upper half of the diagram and the attainable region is indicated by the unshaded bars in the lower half of the diagram. The height of each bar in the feeder region represents the conditional multi-component breakage function $b_{4,10kl}$ where $k$ and $l$ represent any parent bar in the feeder region. The height of each bar in the attainable region represents the value of $a_{m,n\,4\,10}$.

size classes and 12 grade classes which requires $19 \times 12 = 228$ separate Andrews-Mika diagrams, one for each possible combination of $k$ and $l$. In general a theoretical model of the Andrews-Mika diagram is required to generate the appropriate matrices which can be stored before the operation of the comminution equipment can be simulated.

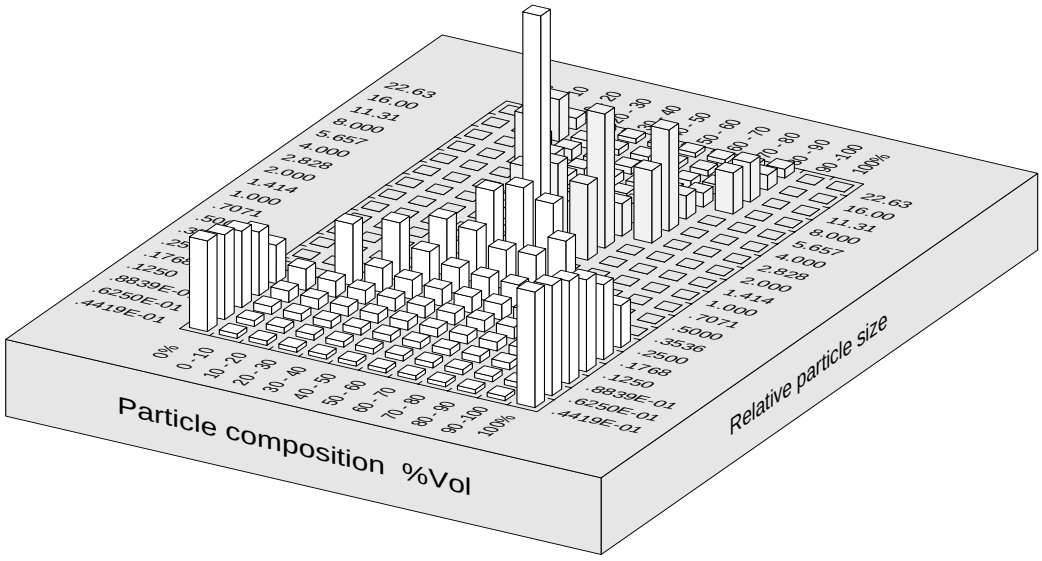


Figure 3.17 Internal structure of a typical Andrews-Mika diagram showing both the feeder and attainable regions. The feeder region is indicated by the shaded bars in the upper half of the diagram and the attainable region is indicated by the unshaded bars in the lower half of the diagram. The height of each bar in the feeder region represents the conditional multi-component breakage function $b_{7,10kl}$ where $k$ and $l$ represent any parent bar in the feeder region. The height of each bar in the attainable region represents the value of $a_{m,n\ 7\ 10}$.

Illustrative example 3.2

Calculate the liberation distribution of progeny particles when parent particles having representative size 3.394 mm and representative grade = 0.504 are broken by random fracture. Assume that the texture is symmetrical and that the liberation size parameter for the ore is 200 μm. Consider two cases: progeny size is 212 μm which is close to the liberation size, and progeny size = 53μm which is considerably smaller than the liberation size.

Values for other parameters in the model are $\delta_o = 2.0$, x = 0.5 , asymmetry factor = 1.0 and $\lambda = 1.0$.

Case 1: Progeny size = 212 μm

Calculate the boundaries of the Andrews-Mika diagram.

$$\delta = \min\left[2.0\left(\frac{200}{3394}\right)^{0.5},\ 3\right] = 0.243$$

Texture is symmetrical, so $\delta_\ell = \delta_u = \delta = 0.243$

The upper boundary is calculated using equation 3.35

$$g_u = \max\left[0.504\left(\frac{3394}{212}\right)^{0.2},\ 0.504\left(\frac{200}{212}\right)^{0.243}\right]$$

$$= \max\,[0.878,\ 0.497]$$

$$= 0.878$$

The lower boundary is calculated using equation 3.36

$$1 - g_\ell = \max\left[0.496\left(\frac{3394}{212}\right)^{0.2},\ 0.496\left(\frac{200}{212}\right)^{0.243}\right]$$

$$= \max\,[0.864,\ 0.489]$$

$$g_\ell = 0.136$$

Both boundaries lie within the range $g = 0$ to $g = 1$, so that the variable $\chi = \dfrac{g - g_\ell}{g_u - g_\ell}$ has a Beta distribution. Thus the cumulative conditional distribution for progeny particles of size 212 μm is

$$P(g|212;\ 0.504,\ 3394) = 0.0 \quad \text{for } g \le g_\ell$$

$$= I_{x(g)}(\alpha,\ \beta) \quad \text{for } g_\ell < g < g_u$$

$$= 1.0 \quad \text{for } g \ge g_u$$

The parameters $\alpha$ and $\beta$ in this distribution are calculated from

$$\alpha = \chi(g)\gamma$$

$$= \frac{0.504 - 0.136}{0.878 - 0.136} \times \gamma$$

$$= 0.496\ \gamma$$

$$\beta = (1 - \chi(g'))\gamma$$

$$= 0.504\ \gamma$$

The parameter $\gamma$ determines the variance of the distribution

$$f(d_p) = \frac{1}{1 + \left(\dfrac{212}{200}\right)^{1.0}} = 0.485$$

$$\gamma = \frac{1 - f(d_p)}{f(d_p)} = \frac{1 - 0.485}{0.485} = 1.061$$

$$\alpha = 0.496 \times 1.061 = 0.526$$

$$\beta = 0.504 \times 1.061 = 0.585$$

Since both $\alpha$ and $\beta$ are less than 1, the distribution is U-shaped, which indicates that the minerals are rapidly approaching liberation as the progeny size passes the mineral grain size.

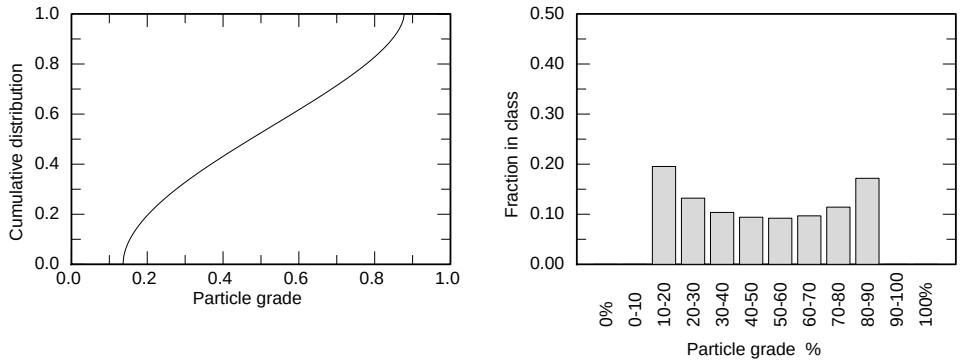


Figure 3.18 Cumulative distribution and histogram of particle grades at progeny size of 212 µm.

The cumulative distribution and the corresponding histogram is shown in Figure 3.18

Case 2: Progeny size = 53 µm

In this case, the boundaries fall outside the range $g = 0$ to $g = 1$ and completely liberated particles will be found in the progeny population.

$$g_u = \max\left[0.501\left(\frac{3394}{53}\right)^{0.2}, 0.504\left(\frac{200}{53}\right)^{0.243}\right]$$

$$= \max[1.158, 0.696]$$

$$= 1.158$$

$$1 - g_\ell = \max\left[0.496\left(\frac{3394}{53}\right)^{0.2}, 0.496\left(\frac{200}{53}\right)^{0.243}\right]$$

$$= \max[1.140, 0.685]$$

$$= 1.140$$

$g_\ell = -0.140$

The liberated factions are calculated from the Beta distribution of the transformed variable,

$$\chi(g) = \frac{g + 0.140}{1.158 + 0.140}$$

which has parameters

$$f(d_p) = \frac{1}{1 + \frac{53}{200}} = 0.791$$

$$\gamma = \frac{1 - 0.791}{0.791} = 0.265$$

$\alpha = g' \gamma = 0.504 \times 0.265 = 0.133$

$\beta = (1 - g') \gamma = 0.496 \times 0.265 = 0.131$

$L_O = I_{\chi(0.0)}(0.133, 0.131) = I_{0.108}(0.133, 0.131)$

$= 0.382$

$L_1 = 1 - I_{\chi(1.0)}(0.133, 0.131) = 1 - I_{0.878}(0.133, 0.131)$

$= 1 - 0.603 = 0.397$

The inner distribution can now be determined.

$\alpha^M = 0.484 \times \gamma = 0.484 \times 0.265 = 0.128$

$\beta^M = (1 - 0.484) \times \gamma = 0.516 \times 0.265 = 0.137$

$$\overline{g}^M = \frac{g' - L_1}{1 - L_O - L_1}$$

$$= \frac{0.504 - 0.397}{1 - 0.382 - 0.397}$$

$= 0.484$

The cumulative conditional distribution for progeny particles of size 53 μm is

$P(g|53; 0.504, 3394) = L_O + (1 - L_O - L_1)\ I_g(0.128, 0.137)$

$= 0.382 + 0.221 \times I_g(0.128, 0.137)$

The cumulative distribution and corresponding histogram are shown in Figure 3.19

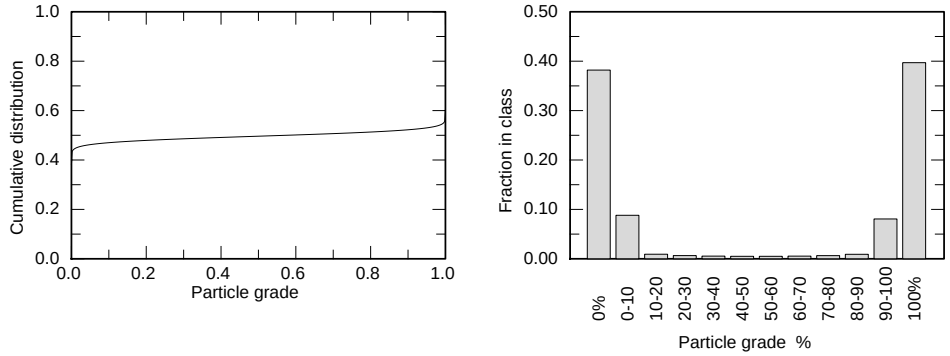


Figure 3.19 Cumulative distribution of particle grades and the corresponding histogram for progeny at 53 μm.

## 10.7 Symbols Used in this Chapter

| | |
|---|---|
| $B(\alpha, \beta)$ | Beta function. |
| $b(d_p:d_p')$ | Breakage function. |
| $b(g,d_p: g',d_p')$ | Breakage function for 2-component material. |
| $d_p$ | Particle size. |
| $D$ | Mesh size. |
| $f(\ell)$ | Distribution density (by length) for intercept length. |
| $f(d_p)$ | Variation of variance with progeny size. |
| $g$ | Mineral grade of particle. |
| $g_L$ | Linear grade. |
| $I_g$ | Incomplete beta function. |
| $\bar{\ell}$ | Average intercept length. |
| $\bar{\ell}_D$ | Average intercept length for particles of size $D$. |
| $L_0$ | Mass fraction of particle population that consists of liberated gangue. |
| $L_1$ | Mass fraction of particle population that consists of liberated mineral. |
| $\mathfrak{L}_0$ | Fraction of available gangue that is liberated. |
| $\mathfrak{L}_1$ | Fraction of available mineral that is liberated. |
| $p(D)$ | Distribution density for particle size. |
| $p(g)$ | Distribution density for particle grade. |
| $p(\ell)$ | Distribution density for intercept length. |
| $p(\ell \mid D)$ | Conditional density for intercept length from particles of size $D$. |
| $p(g_L \mid \ell)$ | Conditional density for linear grades in intercepts of length $\ell$. |
| $\Delta D_R$ | Conditioning variable to indicate particles come from a size interval. |

## 10.8 Bibliography

The importance of mineral liberation and its description in terms of the geometry of the mineralogical texture and the geometrical properties of the particles was analyzed by Gaudin (1939)

using simple geometrical structures. Barbery (1991) gave an account of most of the more recent research up to 1990. Fander (1985) gives a well illustrated account of many mineral textures as seen under the microscope. Jones (1987) provides an excellent account of quantitative methods that are available for the analysis of mineralogical texture. King (1994) has presented an alternative theoretical method for the prediction of mineral liberation from measurements on sections which can be applied when fracture is not random. Andrews and Mika (1976) analyzed the inter-relationship between comminution and liberation using population balance techniques and this forms the basis of the modeling method discussed in this chapter. King (1990) provided a simple model for the internal structure of the Andrews-Mika diagram and Schneider (1995) developed the model to the stage where it could be calibrated using image analysis data obtained from samples of ore.

## 10.9 References


Andrews, J.R.G. and Mika, T.S. (1976) Comminution of heterogeneous material. Development of a model for liberation phenomena. Proc. 11th Int Mineral Processing Congress.

Barbery, G. (1991) Mineral Liberation. Measurement, Simulation and Practical Use in Mineral Processing. Editions GB, Quebec.

Fander, H. W. (1985) Mineralogy for Metallurgists: an Illustrated Guide. The Institution of Mining and Metallurgy, London.

Gaudin, A.M. (1939) Principles of Mineral Dressing. Mc Graw-Hill, New York.

Jones, M. P. (1987) Applied Mineralogy: a Quantitative Approach. Graham and Trotman, London.

King, R.P.(1990) Calculation of the liberation spectrum in products produced in continuous milling circuits. Proc. 7th European symposium on Comminution, Vol 2, pp. 429-444.

King, R. P. (1994) Linear stochastic models for mineral liberation. *Powder Technology*. Vol.81 pp. 217-234

Schneider, C.L. (1995) The Measurement and Calculation of Liberation in Continuous Grinding Circuits. Ph.D Thesis, University of Utah.